Probing the Proton Channel and the Retinal Binding Site of *Natronobacterium pharaonis* Sensory Rhodopsin II

Johann P. Klare,* Georg Schmies,* Igor Chizhov,* Kazumi Shimono,† Naoki Kamo,† and Martin Engelhard*
*Max-Planck-Institut für Molekulare Physiologie, Otto Hahn Strasse 11, D-44227 Dortmund, Germany; and †Laboratory of Biophysical Chemistry, Graduate School of Pharmaceutical Sciences, Hokkaido University, Sapporo 060-0812, Japan

ABSTRACT The sensory rhodopsin II from *Natronobacterium pharaonis* (NpSRII) was mutated to try to create functional properties characteristic of bacteriorhodopsin (BR), the proton pump from *Halobacterium salinarum.* Key residues from the cytoplasmic and extracellular proton transfer channel of BR as well as from the retinal binding site were chosen. The single site mutants L40T, F86D, P183E, and T204A did not display altered function as determined by the kinetics of their photocycles. However, the photocycle of each of the subsequent multisite mutations L40T/F86D, L40T/F86D/P183E, and L40T/F86D/P183E/T204A was quite different from that of the wild-type protein. The reprotonation of the Schiff base could be accelerated ~300- to 400-fold, to approximately two to three times faster than the corresponding reaction in BR. The greatest effect is observed for the quadruple mutant in which Thr-204 is replaced by Ala. This result indicates that mutations affecting conformational changes of the protein might be of decisive importance for the creation of BR-like functional properties.

INTRODUCTION

Phototaxis in Halobacteria is mediated by two receptors, sensory rhodopsin I (SRI) and sensory rhodopsin II (SRII) [also called phoborhodopsin (pR)]. The receptors are responsible for directing the bacteria toward favorable light conditions for the functioning of the two ion pumps bacteriorhodopsin (BR) and halorhodopsin (HR). Whereas BR, HR, and SRI absorb at wavelength above 560 nm, SRII from *H. salinarum* has its absorption maximum at around 490 nm. It is thought that SRII enables the bacteria to accumulate in the dark when the oxygen supply is ample, thus avoiding photooxidative stress (Spudich, 1998).

The amino acid sequence has been determined for all four pigments (a sequence alignment is found in (Seidel et al., 1995)). Structures are now available for all bacterial rhodopsins with the exception of SRI (BR structure reviewed in Lanyi and Luecke (2001)), HR (Kolbe et al., 2000), and NpSRII (Luecke et al., 2001; Royant et al., 2001). The general features of the structures are quite similar with seven transmembrane helices (A to G) situated almost perpendicular to the membrane. The binding pocket of the chromophore (all-*trans* retinal), which is bound via a protonated Schiff base to a lysine residue located on helix G, encompasses several amino acids distributed over all seven helices. Most of these amino acids are conserved within the family of archaeal rhodopsins. Differences in the binding site between SRII and the other three pigments were thought to be responsible for the blue shifted absorption maximum of SRII. However, mutational studies generated only minor effects (Shimono et al., 2000). Even if 10 residues of NpSRII were replaced by those from the corresponding positions in BR a red-shift of only 28 nm was observed (Shimono et al., 2001). Additional blue shift of NpSRII with respect to BR has been attributed to the repositioning of Arg-72 in the chromophore pocket (Luecke et al., 2001).

On excitation by light the retinal chromophore undergoes an all-*trans*→13-*cis* isomerization, which is followed by thermal relaxations. The resulting sequence of intermediates, which finally lead back to the original ground state of the pigment have been denoted in analogy to the BR-nomenclature K, L, M, N, and O state. This reaction cycle (also called photocycle) involves not only the reversal of the isomerization of retinal but also proton transfer steps and conformational changes of the protein (for recent reviews, see Lanyi and Luecke (2001), Spudich et al. (2000), Schäfer et al. (1999), and Shimono et al. (2001)). In the case of BR and HR, where the cycletime is $<$100 ms, ion pumping is effective. On the other hand SRI and SRII with turnover times of $>$1 s are inefficient proton pumps especially under the conditions of a high membrane potential (Schmies et al., 2001) as it is experienced by *H. salinarum* and *N. pharaonis* (Michel and Oesterhelt, 1980; Wittenberg, 1995).

The amino acid sequences of SRII from *H. salinarum* (HsSRII or HspR) and *N. pharaonis* (NpSRII or NppR) have been determined (Zhang et al., 1996; Seidel et al., 1995). Their sequence homology is ~53%. Also the photocycles of the two pigments are quite comparable, and it has been deduced that NpSRII is an adequate model system for the *H. salinarum* receptor HsSRII (Scharf et al., 1992).

In BR and NpSRII the corresponding residues involved in the proton release and uptake pathways are in part conserved with some notable exceptions. For example, in the extracellular channel Glu-194, which is involved in the final proton release (Balashov et al., 1997) is replaced by Pro-183 in NpSRII. Other important residues from the cytoplasmic channel are Thr-46^{BR}→Leu-40^{NpSRII} and Asp-96^{BR}→Phe-86^{NpSRII}. The carbonyl of Ala-215^{BR} forms a hydrogen

Submitted September 25, 2001, and accepted for publication December 11, 2001.

Address reprint requests to M. Engelhard, Max-Planck-Institut für Molekulare, Physiologie, Otto Hahn Strasse 11, D-44227, Germany. Tel.: 49-231-1332302; Fax: 49-231-1332399; E-mail: martin.engelhard@mpi-dortmund.mpg.de.

0006-3495/02/04/2156/09 $2.00

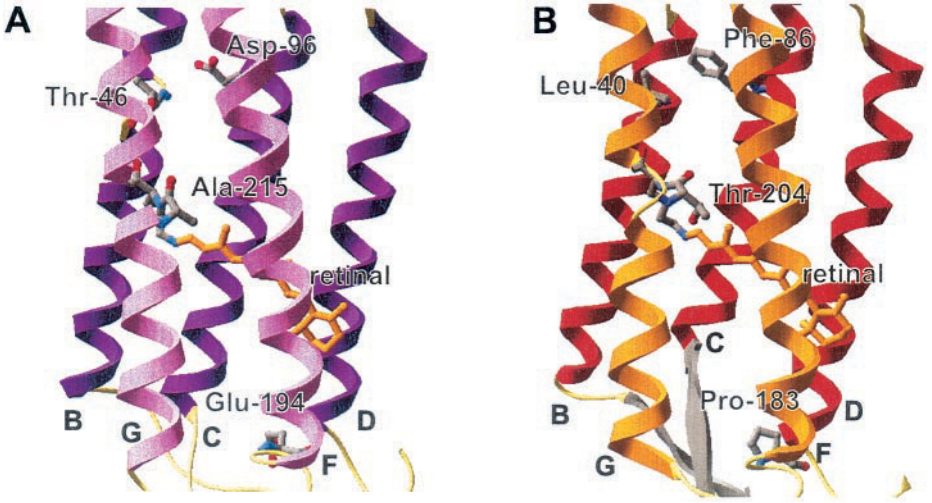

FIGURE 1 Portions of the crystal structures of BR (*A*) and NpSRII (*B*) as ribbon presentation showing the amino acids at the sites of mutation. The structures were taken from the protein data bank (BR, 1C3W; NpSRII, 1JGJ).

bond to a water molecule bridging to the indole nitrogen of Trp-182^{BR}. This interaction is disrupted by the transition to the M state (Lanyi and Luecke, 2001). In NpSRII, Ala-215^{BR} is replaced by the bulkier Thr-204^{NpSRII}, which might influence the L→M transition. The slow turnover of the NpSRII photocycle (Chizhov et al., 1998) has been attributed to the altered charge distribution in the cytoplasmic channel (Iwamoto et al., 1999a). Indeed, the addition of a proton donor group like azide increased the rate of M-decay considerably. Also the introduction of an carboxyl-group as in the F86D showed a similar effect, albeit less pronounced (Iwamoto et al., 1999a; Takao et al., 1998; Schmies et al., 2000).

The hydrogen bond network of the proton release channel in BR is probably disrupted in NpSRII, most importantly by the replacement of Glu-194^{BR} by Pro-183^{NpSRII}. The disturbance of this functional unit might explain the retarded proton release, which occurs after the capture of another proton from the cytoplasm and/or extracellular side. The latter uptake site would lead to a futile proton pump (Sasaki and Spudich, 1999; Sudo et al., 2001).

To assign those amino acids, which convert the slow photocycling NpSRII into a fast cycling pigment, several residues from the retinal binding pocket, the cytoplasmic channel, and the extracellular channel were mutated to those of BR. As expression system *Escherichia coli* has been chosen because of the ease and speed of genetic manipulation. Furthermore, *N. pharaonis* is not accessible for transformation and selection. Amino acids selected from the retinal binding site were altered at 10 positions (I43V/I83L/N105D/V108M/M109I/F127W/G103S/A131T/F134M/T204A). From the proton transfer channels L40T, F86D, P183E, and T204A mutants were constructed (see Fig. 1 for the positions of the mutation sites) as well as double (L40T/F86D), triple (L40T/F86D/P183E), and quadruple mutants (L40T/F86D/P183E/T204A). The analysis of the photocycles of these mutants provide information about the key-groups modulating the M→O reaction pathway.

MATERIALS AND METHODS

All reagents used were of analytical grade.

Bacterial strains

For DNA manipulation *E. coli* XL1 was used. *E. coli* strain BL21 (DE3) was used for gene expression. Cells were grown in Luria-Bertani medium containing 50 μg/ml Kanamycin.

Preparation of NpSRII mutants

For the construction of the mutated C-terminal 7× His-tagged *NpsopII* genes the plasmid pET27bmod (Klostermeier et al., 1998) derived from pET27b (Novagen, Madison, WI) was used. The *NpsopII*-mutants (*NpsopII* L40T, *NpsopII*-F86D, *NpsopII*-P183E, *NpsopII*-T204A, *NpsopII*-L40T/F86D, *NpsopII*-L40T/F86D/P183E, and *NpsopII*-L40T/F86D/P183E/T204A) were prepared by polymerase chain reaction using the overlap-extension method (Higuchi et al., 1988; Ho et al., 1989). *E. coli* cells were transformed by electroporation (Dower et al., 1988). L40T-NpSRII, F86D-NpSRII, P183E-NpSRII, T204A-NpSRII, L40T/F86D-NpSRII, L40T/F86D/P183E-NpSRII, and L40T/F86D/P183E/T204A-NpSRII were expressed according to Shimono et al. (1997) and purified using the method of Hohenfeld et al. (1999). The 10-fold mutant (I43V/I83L/N105D/V108M/M109I/F127W/G103S/A131T/F134M/T204A-NpSRII) was expressed and purified as described (Shimono et al., 2001).

Reconstitution into purple membrane lipids

The solubilized proteins were reconstituted into native purple membrane (PM) lipids by incubation for 16 h in a buffer (300 mM NaCl, 50 mM NaH_2PO_4/Na_2HPO_4, pH 7.2) containing a 15-fold excess of lipids and detergent-absorbing biobeads (100 mg biobeads/mg protein; Biorad, München, Germany). After filtration the protein-containing membrane lipids were pelleted by centrifugation (100,000 × *g*, 1 h, 4°C) and resuspended in 150 mM Nacl, 10 mM Tris·HCl, pH 8.0).

Laser flash photolysis and data analysis

The photocycle experiments and the analysis of the data were done as described by Chizhov and coworkers (Chizhov et al., 1996, 1998; Chizhov and Engelhard, 2001).

For the quadruple mutant (L40T/F86D/P183E/T204A-NpSRII) an extended data set was measured including different temperatures ranging from 10°C to 55°C in steps of 5°C and wavelength scan ranging from 360 to 660 nm. Analysis of the whole data set was carried out using the global nonlinear multiexponential fitting program (MEXFIT) (Chizhov et al., 1996; Müller and Plesser, 1991). Each temperature point was treated independently.

pH dependence of quadruple mutant

For the measurement of the pH dependence the quadruple mutant was reconstituted into PM lipids and subsequently immobilized in a 16.5% acrylamide gel. Before the photocycle measurements the gel slice was equilibrated with the appropriate buffer (150 mM NaCl, 10 mM Tris, pH ranging from 5 to 12.1) for at least 15 min. Traces were collected at 400, 500, and 550 nm.

RESULTS

Photocycle turnover

The flash-induced absorption changes at representative wavelengths of the single-site mutants NpSRII-L40T, NpSRII-F86D, NpSRII-P183E, and NpSRII-T204A are shown in Fig. 2. The photocycle of the other samples, NpSRII, L40T/F86D-NpSRII, L40T/F86D/P183E-NpSRII, L40T/F86D/P183E/T204A-NpSRII as well as the 10-fold mutant are shown in Fig. 3. Depletion and recovery of the ground state was monitored at 500 nm, whereas the traces at 400 and 550 nm represent rise and decay of the M-like and O-like intermediates, respectively. The corresponding kinetic data, i.e., M rise, M decay/O rise, and O decay are summarized in Table 1. It is obvious that the photocycle turnover rate is quite similar for most of the mutated proteins. For the single site- and the 10-site mutants ~75% of the receptor molecules have completed their photocycles after 1 s. Only the triple and quadruple mutants display an accelerated turnover. However, even the photocycle of the quadruple mutant is one order of magnitude slower than that of BR. It should be noted that the introduction of Ala in position 204 (T204A) slows down the photocycle even further if compared with that of the wild type. Concomitantly, the transient amplitude of the O intermediate is reduced considerably. The turnover of the 10-site mutant is almost identical to that of the wild-type NpSRII.

Single-site mutants

The photocycles of all single site mutants are generally almost identical to that of wild-type NpSRII and do not show any differences in the turnover rate (Fig. 2). However, minor differences are noticeable for all four mutants. F86D-NpSRII shows an accelerated M decay (Table 1), in agreement with previous results (Iwamoto et al., 1999a). NpSRII-T204A displays a decay of the M-like form approximately three times slower than that for the wild type. All mutants except F86D-NpSRII exhibit a reduced transient concentration of O as depicted by the traces measured at 550 nm (Fig. 2). It is also interesting to note that for T204A-NpSRII the M rise is accelerated by a factor of 2 (Fig. 2 *D*; Table 1). This observation is also true for the multisite mutants possessing the same amino acid exchange, i.e., the quadruple- and the 10-site mutant (see Table 1).

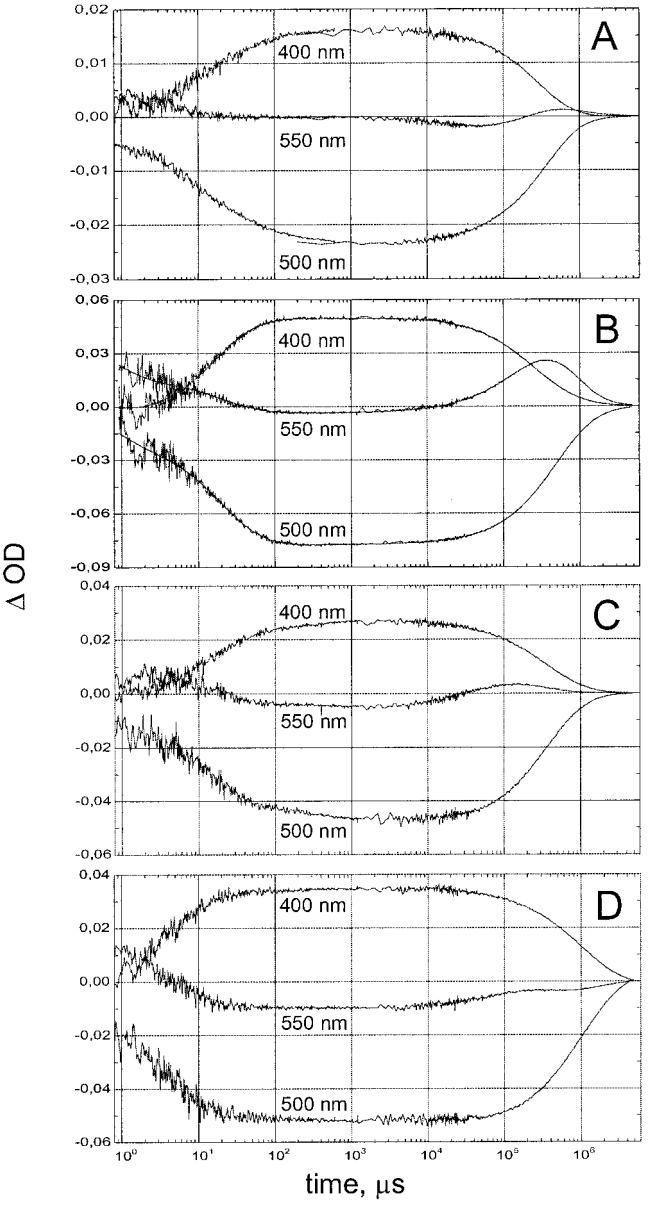

FIGURE 2 Photocycles of the single-site mutants measured at 25°C (150 mM NaCl, 10 mM Tris HCl, pH 8). Absorbance changes are depicted for 400, 500, and 550 nm. (*A*) L40T-NpSRII, (*B*) F86D-NpSRII, (*C*) P183E-NpSRII, (*D*) T204A-NpSRII.

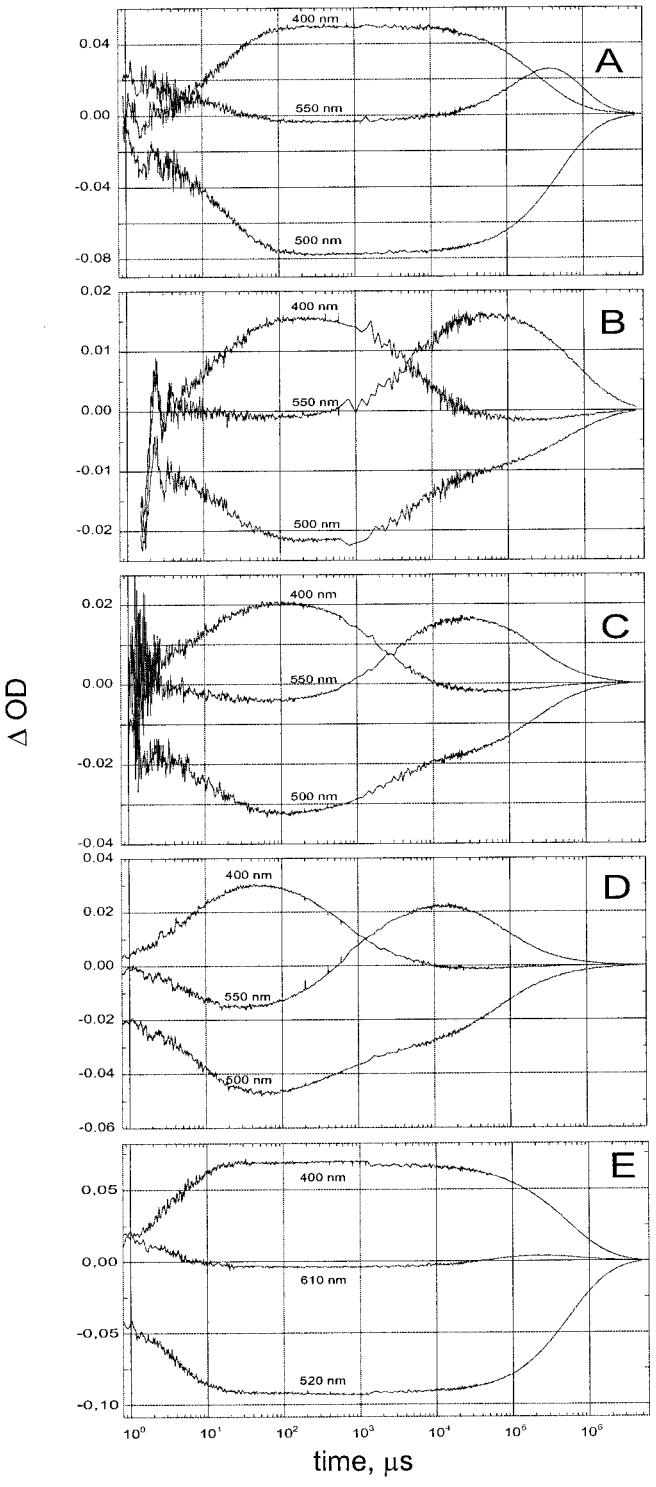

FIGURE 3 Photocycles of NpSRII, the three channel-mutants, and the retinal binding pocket-mutant measured at 25°C (150 mM NaCl, 10 mM Tris HCl, pH 8). Absorbance changes are depicted for 400, 500, and 550 nm for NpSRII and its channel-mutants, and 410, 520, and 610 nm for the 10-fold mutant. These wavelength are characteristic for the formation and decay of the M-like, parent-, and O-like state, respectively. (*A*) NpSRII, (*B*) L40T/F86D-NpSRII, (*C*) L40T/F86D/P183E-NpSRII, (*D*) L40T/F86D/P183E/T204A-NpSRII, (*E*) I43V/I83L/N105D/V108M/M109I/F127W/G103S/A131T/F134M/T204A-NpSRII.

TABLE 1 Kinetic data of single- and multi-site mutants

Sample	M rise	M decay/ O rise	O decay	Cycle completed after 1 s
NpSRII	12 μs	150 ms	400 ms	75%
L40T	8 μs	90 ms	400 ms	76%
F86D	10 μs	120 ms	500 ms	70%
P183E	12 μs	250 ms	400 ms	76%
T204A	6 μs	500 ms	—*	69%
L40T/F86D	8 μs	6 ms	300 ms	85%
L40T/F86D/P183E	12 μs	3 ms	160 ms	96%
L40T/F86D/P183E/T204A	7 μs	0.5 ms	40 ms	99%
BR†	30 μs	1.2 ms	4 ms	100%‡
10-site mutant	6 μs	150 ms	400 ms	75%

Measured at 25°C (150 mM NaCl, 10 mM Tris HCl, pH 8).
*Could not be determined because of weak transient amplitude of O-like form (see Fig. 2 *D*).
†Data taken from Chizhov et al., 1996.
‡Cycle completed already after 100 ms.

L40T/F86D-NpSRII

If the two cytoplasmic-channel residues Leu-40 and Phe-86 are both replaced by Thr and Asp, respectively, the photocycle kinetics are considerably altered (Fig. 3 *B*). Whereas, the M-state formation is not affected, the M decay is accelerated by a factor of ~25, an observation that was also made by Iwamoto et al. (1999a). For BR the M decay takes place in the same time window. Concomitantly with the M decay, O_{550} is formed at an ~25 times faster rate than that of NpSRII. However, the recovery of the ground state, which is coupled to the decay of O_{550}, is not significantly accelerated. As a consequence, the transient concentration of O_{550} is increased as indicated by the higher amplitude of the corresponding trace at 550 nm (Fig. 3 *B*).

L40T/F86D/P183E-NpSRII

An additional replacement of Pro-183 by Glu located in the extracellular channel (Fig. 3 *C*) affects the formation as well as decay of the M-like intermediate by a factor of ~2, as compared with the double mutant. The formation and the decay of the O-like species is also slightly altered, leading to a turnover rate of the photocycle, which is approximately two times faster compared with that of NpSRII.

L40T/F86D/P183E/T204A-NpSRII

The additional substitution of Thr-204 by Ala (Fig. 3 *D*) results in a further acceleration of the reprotonation of the Schiff base leading to a two- to threefold increase in the decay of the M-like intermediate as compared with the corresponding rate in the photocycle of BR. The formation of the O-like species is accelerated by a factor of 4 to 5 (compared with that of the triple mutant), as well as its

decay is approximately four times faster. However, the recovery of the ground state, characterized by the trace at 500 mm, is not accelerated. Another consequence of this mutation is a bathochromic shift of the absorption maximum from 500 nm (wt-NpSRII) to 509 nm.

I43V/I83L/N105D/V108M/M109I/F127W/G103S/A131T/F134M/T204A-NpSRII

The light-induced transient absorption changes of the retinal binding pocket-mutant are shown in Fig. 3 *E*. Depletion and recovery of the initial state are monitored at 520 nm, corresponding to the shifted absorption maximum at 528 nm. The trace at 410 nm represents formation and decay of the M-like state, whereas the record at 610 nm corresponds to the rise and decay of the O-like intermediate. As already mentioned, the photocycle turnover rate of this mutant is the same as that of the wild-type receptor. In contrast to that, the M-like intermediate is formed approximately five times faster, and its decay is slowed down by a factor of approximately two to three. This results in a significantly prolonged residence time of the M-like state. The O-like form seems to have a faster decay, and its amplitude is ~5 to 10 times smaller as compared with that of NpSRII.

Detailed analysis of the L40T/F86D/P183E/T204A-NpSRII photocycle

The photocycle data of the mutants revealed for the quadruple mutant the most pronounced effects. To investigate the properties of this mutant in further detail its kinetics were studied over a wider set of parameters. Photocycle data were collected for temperatures ranging from 10°C to 55°C. At each temperature point the wavelength was varied between 360 and 660 nm. The analysis was again performed by using a unidirectional sequential model of irreversible first-order reactions (Chizhov et al., 1996, 1998).

The photocycle kinetics of the quadruple mutant can be described by seven exponentials (τ_1–τ_7) if the temperature does not exceed 30°C. At higher temperatures the fastest time constant (τ_1) cannot be resolved. The Arrhenius plot of the apparent rate constants of the quadruple mutant is shown in Fig. 4. The corresponding apparent activation parameters are given in Table 2.

The absolute absorbance spectra of the kinetic states (P_1–P_7, data not shown) were obtained by adding the differential spectra (data not shown) to the initial spectrum (Fig. 5) of the quadruple mutant. The parameters of the multi-Gaussian fit used to approximate the absolute spectrum of the initial state are shown in Table 3. The spectra of the kinetic states P_1 and P_3 do have a single maximum at 520 and 400 nm, respectively, and are almost temperature independent. They can be interpreted

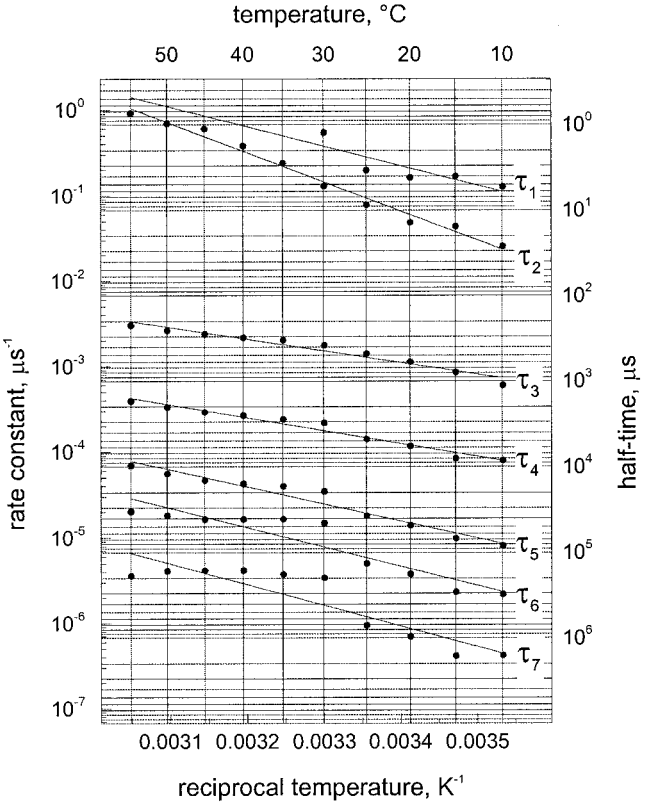

FIGURE 4 Temperature dependence of the apparent rate constants derived from a seven-exponential global fit of the L40T/F86D/P183E/T204A mutant. Rate constants shown in the Arrhenius plot were determined at pH 8.0. Straight lines represent the least-squares fit of the apparent activation parameters (see Table 2) according to the Eyring equation. The horizontal grid lines correspond to the right (half times) axis, the vertical grid lines correspond to the top (°C) axis.

as pure spectral intermediates. By comparison with the intermediates of the NpSRII photocycle (Chizhov et al., 1998) they can be assigned to K- and M-like intermediates. The spectra of the other states (P_2, P_4, P_5, and P_6) are temperature dependent and represent equilibria between different spectral states. P_2 shows equilibrium between M and an L-like species absorbing at 490 nm, whereas P_4 and P_5 display equilibria between M and an O-like species (absorbing at 560 nm). At higher temperatures this equilibrium is shifted in favor of O_{560}.

Comparing this data with those from the photocycle kinetics of NpSRII, it is obvious that the general mechanism has not changed. Both, NpSRII and its quadruple mutant reveal a pure M-state with preceding M↔ L and subsequent M↔ O, N equilibria. The major difference concerns the spectrally silent transition between two M states in NpSRII, which is not detected in the quadruple mutant, probably because of kinetic reasons. Thus, the sequential effects of the mutations can be directly compared with single steps within the NpSRII photocycle.

TABLE 2 Apparent activation parameters of the L40T/F86D/P183E/T204A-NpSRII photocycle

	τ_1	τ_2	τ_3	τ_4	τ_5	τ_6	τ_7
$\Delta H^{\#}$ (kJ/mol)	41 ± 16	63 ± 3	24 ± 2	26 ± 2	35 ± 3	41 ± 6	44 ± 8
$\Delta S^{\#}$ (J/mol K)	−2 ± 52	61 ± 9	−106 ± 7	−115 ± 6	−101 ± 10	−94 ± 20	−96 ± 25

pH dependency of the L40T/F86D/P183E/T204A-NpSRII photocycle

The photocycle of the quadruple mutant is not altered in a pH range between pH 5 and 8.1. Contrary to the M rise, the M decay is substantially retarded by increasing the pH (Fig. 6). Furthermore, the transient amplitude of O becomes negligible (data not shown). The kinetics of the M decay can be described satisfactorily by three exponentials. The dependency of the major component of the M decay on pH was fitted using the Michaelis-Menten equation, which gave a pK_a of 9.5 ± 0.2. For comparison, wild-type NpSRII has an apparent pK_a above 10.5 (data not shown). It is interesting to note that HsSRII displays an apparent pK_a of ~7.5 (Sasaki and Spudich, 1999), which was attributed to an unidentified group XH. Compared with NpSRII the quadruple mutant has a much lower pK, indicating that instead of XH, Asp-86 is titrated.

DISCUSSION

After photoexitation, BR undergoes a multistep reaction cycle during which a proton is transferred from the cytoplasm to the extracellular side of the membrane. In a general perspective these reactions comprise retinal isomerization, protein conformational changes (helix F movement), and proton transfer reactions (proton release and proton uptake). All three processes have been proven to occur also in NpSRII after light excitation. The reisomerization of 13-*cis* retinal to its all-*trans* configuration occurs with the formation of the O intermediate (F. Siebert, personal communication). Proton transfer steps are connected to the release and uptake of protons (Sudo et al., 2001; Iwamoto et al., 1999b; Sasaki and Spudich, 2000; Engelhard et al., 1996; Schmies et al., 2001) Finally, an outwardly directed movement of helix F has been shown by electron paramagnetic resonance experiments (Wegener et al., 2000).

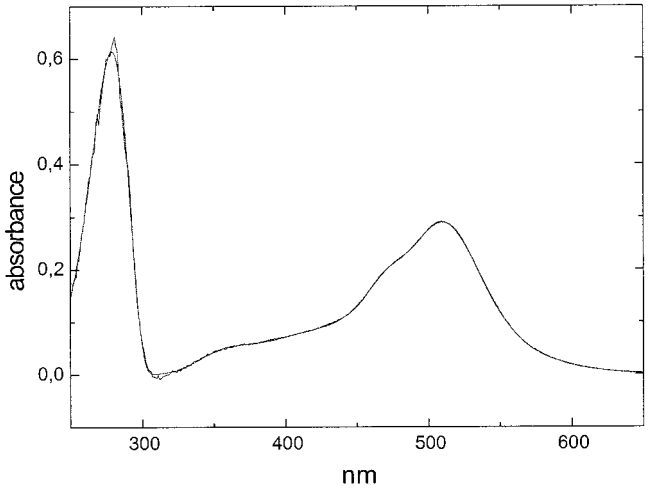

FIGURE 5 Absolute spectrum and fit of the L40T/F86D/P183E/T204A mutant reconstituted into PM lipids taken at room temperature. Effects of light-scattering were subtracted according to Chizhov et al. (1998).

The main differences between NpSRII and BR are related to the turnover of the photocycle and the relative time course of the processes connected to the protonation/deprotonation of functional important amino acids as well as the conformational changes of the protein. Most importantly, in NpSRII an N-like intermediate is barely detectable (Chizhov et al., 1998). Furthermore, unlike in BR, the proton uptake precedes the proton release in SRII (Sasaki and Spudich, 2000; Iwamoto et al., 1999b). Another difference might be found in the time scale of the flab-like movement of helix F, which in NpSRII is likely to take place with the formation of M (or earlier). This conclusion was drawn from electron paramagnetic resonance-experiments, which had a time resolution of 3 ms (Wegener et al., 2000). In selected experiments the time resolution was increased to 1 ms (Wegener, 2000). In both sets of experiments the ESR-transient, which correlated to the movement of helix F is already fully evolved at the earliest time points. Because in NpSRII the M_1 to M_2 transition occurs with 2 ms one could argue that the flab-like motion of helix F is correlated at least with the formation of M. For comparison, the helix F movement in BR has been attributed to the formation of the M_2 intermediate (Subramaniam and Henderson, 2000; Radzwill et al., 2001).

In principle, BR-like properties induced in NpSRII should be obtained by replacing those functional relevant amino acids that differ from BR. A step-by-step exchange should provide information about the functional role of

TABLE 3 Parameters of the Gaussian fit of the chromophore spectra of the ground state of L40T/F86D/P183E/T204A-NpSRII

	OD	ρ	$\Delta\nu$ (cm^{-1})	λ_{max} (nm)
S_{01}	1.00 ± 0.07	1.03 ± 0.65	2501 ± 373	509.0 ± 5.0
S_{02}	0.36 ± 0.02	1.54 ± 0.62	2102 ± 1629	463.3 ± 15.5
S_{03}	0.22 ± 0.02	1.25 ± 2.08	4051 ± 3126	414.7 ± 42.0
S_{04}	0.14 ± 0.01	1.00 ± 0.28	3906 ± 1753	358.9 ± 14.9

sd = 0.014.

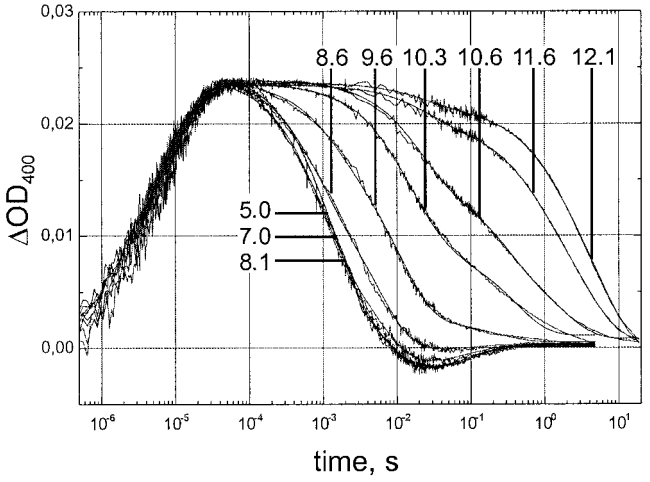

FIGURE 6 pH dependency of the absorbance changes at 400 nm corresponding to the M intermediate of L40T/F86D/P183E/T204A mutant reconstituted into PM lipids at 25°C and immobilized in a polyacrylamide gel. Thin solid lines represent the result of the three-exponential fit.

individual residues. In a first set of experiments single site mutants were analyzed. The results clearly show that each of these mutants have almost no influence on the photocycle. Only with the introduction of a second BR-like site into the cytoplasmic channel is a significant acceleration of the M decay/O rise observed indicating a synergistic effect of the mutations. The half-life time of 6 ms is in the same time range as the M decay in BR, which is ~1.2 ms. Apparently, these two mutations (L40T/F86D) are sufficient to optimize the proton transfer from Asp-86 to the Schiff base that occurs during the $M_2 \rightarrow N$ transition (for a recent review on the protonation reactions and their coupling in BR, see Balashov (2000)). Because in NpSRII the kinetic of the O rise is almost identical to the M decay, the transient concentration of the N intermediate is negligible. This observation indicates that Asp-86 reprotonates (unlike Asp-96 in BR) almost at the same time as the Schiff-base receives its proton. The reason that O formation and M decay occur at the same time could be related to the opening of the cytoplasmic channel with the formation of M_1 or M_2. An indication for this conclusion is the observation that the pK_a related to the M decay drops from 11.5 in NpSRII to 9.5 in the quadruple mutant.

Obviously, the double mutation affects dominantly the $M \rightarrow N \rightarrow O$ sequence of the intermediates. However, the faster M decay is not accompanied by a considerable higher turnover number as indicated by the half time of the O decay and the completion of the photocycle after 1 s (see Table 1). According to recent results (Sasaki and Spudich, 1999; Iwamoto et al., 1999b), a proton is released to the extracellular medium only in the last step of the photocycle. This observation has been related to amino acids within the extracellular channel, which disturb the hydrogen bonded network described for BR (Rammelsberg et al., 1998; Luecke et al., 1999b). To adjust also the proton release kinetics and the turnover of NpSRII to values typical for BR, a third mutation was introduced. In the extracellular channel of BR two sites (Glu-194 and Glu-204) are intimately involved in the mechanism of proton release (Lu et al., 2000; Balashov et al., 1999; Rammelsberg et al., 1998; Luecke et al., 2000). In NpSRII these groups are substituted by Pro-183 and Asp-193, respectively. Because Asp-193 and Glu-204 are homologous amino acids bearing both a carboxyl group function, the P183 was chosen for an additional mutation into a Glu residue (P183E). As can be seen from Table 1 the triple mutant (L40T/F86D/P183E) displays a further acceleration of the M decay but only a slightly increased turnover. Obviously, the lifetime of the O intermediate is not considerably affected by this additional mutation.

Interestingly, if a further exchange is made at a position not directly involved in the proton transfer paths, the O decay is accelerated by a factor of 10 compared with wild type (40 ms vs. 400 ms). Ala-215^{BR} forming the π-bulge at the retinal binding site on helix G is connected via a water molecule to the indole nitrogen of Trp-182. This interaction is disrupted in the M intermediate (Luecke et al., 1999a; Sass et al., 2000). In NpSRII Ala-215^{BR} is replaced by a Thr ($T204^{NpSRII}$), which similarly forms the same water mediated hydrogen bond to a Trp residue ($W171^{NpSRII}$) (Luecke et al., 2001; Royant et al., 2001). Obviously, the bulkier side chain of a Thr residue as compared with Ala not only influences the M-rise (as was demonstrated by the kinetics of the mutants containing the Thr→Ala exchange) but also the later part of the photocycle. This latter result indicates that the optimization of the proton release and uptake pathways is not solely a matter of the groups directly involved. Properties such as dynamics of the protein or overall charge distribution might also play an important role for the optimization of the light activated reactions. This conclusion is in line with the observation that an extensive mutation in the retinal binding site of NpSRII does not lead to a spectral shift as expected for an BR-like retinal environment (Shimono et al., 2001).

In the present work we have shown that the reprotonation of the Schiff base from the cytoplasm can be influenced and accelerated by mutating two amino acids (L40T and F86D) located in the cytoplasmic channel. However, the proton release pathway can only be partly tuned to adapt the corresponding characteristics of BR. The main effect is observed on exchanging Thr-204 by an alanine residue indicating that conformational changes of the protein are rate limiting steps in the photocycle. For a complete transformation of the functional properties of NpSRII into those of BR, additional mutations have to be introduced at presently unknown and uncharacterized sites. The very nature of NpSRII as a photoreceptor might be a reason that it is relatively robust against alterations of its primary sequence.

REFERENCES

Balashov, S. P. 2000. Protonation reactions and their coupling in bacteriorhodopsin. *Biochim. Biophys. Acta Bioenerg.* 1460:75–94.

Balashov, S. P., E. S. Imasheva, T. G. Ebrey, N. Chen, D. R. Menick, and R. K. Crouch. 1997. Glutamate-194 to cysteine mutation inhibits fast light-induced proton release in bacteriorhodopsin. *Biochemistry.* 36: 8671–8676.

Balashov, S. P., M. Lu, E. S. Imasheva, R. Govindjee, T. G. Ebrey, B. Othersen, Y. M. Chen, R. K. Crouch, and D. R. Menick. 1999. The proton release group of bacteriorhodopsin controls the rate of the final step of its photocycle at low pH. *Biochemistry.* 38:2026–2039.

Chizhov, I., D. S. Chernavskii, M. Engelhard, K. H. Müller, B. V. Zubov, and B. Hess. 1996. Spectrally silent transitions in the bacteriorhodopsin photocycle. *Biophys. J.* 71:2329–2345.

Chizhov, I. and M. Engelhard. 2001. Temperature and halide dependence of the photocycle of halorhodopsin from *Natronobacterium pharaonis. Biophys. J.* 81:1600–1612.

Chizhov, I., G. Schmies, R. Seidel, J. R. Sydor, B. Lüttenberg, and M. Engelhard. 1998. The photophobic receptor from *Natronobacterium pharaonis*: temperature and pH dependencies of the photocycle of sensory rhodopsin II. *Biophys. J.* 75:999–1009.

Dower, W. J., J. F. Miller, and C. W. Ragsdale. 1988. High efficiency transformation of *E. coli* by high voltage electroporation. *Nucleic Acids Res.* 16:6127–6145.

Engelhard, M., B. Scharf, and F. Siebert. 1996. Protonation changes during the photocycle of sensory rhodopsin II from *Natronobacterium pharaonis. FEBS Lett.* 395:195–198.

Higuchi, R., B. Krummel, and R. K. Saiki. 1988. A general method of in vitro preparation and specific mutagenesis of DNA fragments: study of protein and DNA interactions. *Nucleic Acids Res.* 16:7351–7367.

Ho, S. N., H. D. Hunt, R. M. Horton, J. K. Pullen, and L. R. Pease. 1989. Site-directed mutagenesis by overlap extension using the polymerase chain reaction. *Gene.* 77:51–59.

Hohenfeld, I. P., A. A. Wegener, and M. Engelhard. 1999. Purification of histidine tagged bacteriorhodopsin, *pharaonis* halorhodopsin, and *pharaonis* sensory rhodopsin II functionally expressed in *Escherichia coli. FEBS Lett.* 442:198–202.

Iwamoto, M., K. Shimono, M. Sumi, and N. Kamo. 1999a. Positioning proton-donating residues to the Schiff-base accelerates the M-decay of *pharaonis* phoborhodopsin expressed in *Escherichia coli. Biophys. Chem.* 79:187–192.

Iwamoto, M., K. Shimono, M. Sumi, K. Koyama, and N. Kamo. 1999b. Light-induced proton uptake and release of *pharaonis* phoborhodopsin detected by a photoelectrochemical cell. *J. Phys. Chem. B.* 103: 10311–10315.

Klostermeier, D., R. Seidel, and J. Reinstein. 1998. Functional properties of the molecular chaperone DnaK from *Thermus thermophilus. J. Mol. Biol.* 279:841–853.

Kolbe, M., H. Besir, L. O. Essen, and D. Oesterhelt. 2000. Structure of the light-driven chloride pump halorhodopsin at 1.8 Å resolution. *Science.* 288:1390–1396.

Lanyi, J. K., and H. Luecke. 2001. Bacteriorhodopsin. *Curr. Opin. Struct. Biol.* 11:415–419.

Lu, M., S. P. Balashov, T. G. Ebrey, N. Chen, Y. Chen, D. R. Menick, and R. K. Crouch. 2000. Evidence for the rate of the final step in the bacteriorhodopsin photocycle being controlled by the proton release group: R134H mutant. *Biochemistry.* 39:2325–2331.

Luecke, H., B. Schobert, J. P. Cartailler, H. T. Richter, A. Rosengarth, R. Needleman, and J. K. Lanyi. 2000. Coupling photoisomerization of retinal to directional transport in bacteriorhodopsin. *J. Mol. Biol.* 300: 1237–1255.

Luecke, H., B. Schobert, J. K. Lanyi, E. N. Spudich, and J. L. Spudich. 2001. Crystal structure of sensory rhodopsin II at 2.4 Angstroms: insights into color tuning and transducer interaction. *Science.* 293: 1499–1503.

Luecke, H., B. Schobert, H. T. Richter, J. P. Cartailler, and J. K. Lanyi. 1999a. Structural changes in bacteriorhodopsin during ion transport at 2 Ångstrom resolution. *Science.* 286:255–261.

Luecke, H., B. Schobert, H. T. Richter, J. P. Cartailler, and J. K. Lanyi. 1999b. Structure of bacteriorhodopsin at 1.55 Ångstrom resolution. *J. Mol. Biol.* 291:899–911.

Michel, H. and D. Oesterhelt. 1980. Electrochemical proton gradient across the cell membrane of *Halobacterium halobium*: effect of *N*,*N*′-dicyclohexylcarbodiimide, relation to intracellular adenosine triphosphate, adenosine diphosphate, and phosphate concentration, and influence of the potassium gradient. *Biochemistry.* 19:4607–4614.

Müller, K.-H. and Th. Plesser. 1991. Variance reduction by simultaneous multi-exponential analysis of data sets from different experiments. *Eur. Biophys. J.* 19:231–240.

Radzwill, N., K. Gerwert, and H.-J. Steinhoff. 2001. Time-resolved detection of transient movement of helices F and G in doubly spin-labeled bacteriorhodopsin. *Biophys. J.* 80:2856–2866.

Rammelsberg, R., G. Huhn, M. Lübben, and K. Gerwert. 1998. Bacteriorhodopsins intramolecular proton-release pathway consists of a hydrogen-bonded network. *Biochemistry.* 37:5001–5009.

Royant, A., P. Nollert, R. Neutze, E. M. Landau, E. Pebay-Peyroula, and J. Navarro. 2001. X-ray structure of sensory rhodopsin II at 2.1-A resolution. *Proc. Natl. Acad. Sci. U. S. A.* 98:10131–10136.

Sasaki, J. and J. L. Spudich. 1999. Proton circulation during the photocycle of sensory rhodopsin II. *Biophys. J.* 77:2145–2152.

Sasaki, J. and J. L. Spudich. 2000. Proton transport by sensory rhodopsins and its modulation by transducer binding. *Biochim. Biophys. Acta.* 1460:230–239.

Sass, H. J., G. Büldt, R. Gessenich, D. Hehn, D. Neff, R. Schlesinger, J. Berendzen, and P. Ormos. 2000. Structural alterations for proton translocation in the M state of wild- type bacteriorhodopsin. *Nature.* 406: 649–653.

Schäfer, G., M. Engelhard, and V. Müller. 1999. Bioenergetics of the archaea. *Microbiol. Mol. Biol. Rev.* 63:570–620.

Scharf, B., B. Pevec, B. Hess, and M. Engelhard. 1992. Biochemical and photochemical properties of the photophobic receptors from *Halobacterium halobium* and *Natronobacterium pharaonis. Eur. J. Biochem.* 206:359–366.

Schmies, G., M. Engelhard, P. G. Wood, G. Nagel, and E. Bamberg. 2001. Electrophysiological characterization of specific interactions between bacterial sensory rhodopsins and their transducers. *Proc. Natl. Acad. Sci. U. S. A.* 98:1555–1559.

Schmies, G., B. Lüttenberg, I. Chizhov, M. Engelhard, A. Becker, and E. Bamberg. 2000. Sensory rhodopsin II from the haloalkaliphilic *Natronobacterium pharaonis*: light-activated proton transfer reactions. *Biophys. J.* 78:967–976.

Seidel, R., B. Scharf, M. Gautel, K. Kleine, D. Oesterhelt, and M. Engelhard. 1995. The primary structure of sensory rhodopsin II: a member of an additional retinal protein subgroup is coexpressed with its transducer, the halobacterial transducer of rhodopsin II. *Proc. Natl. Acad. Sci. U. S. A.* 92:3036–3040.

Shimono, K., Y. Ikeura, Y. Sudo, M. Iwamoto, and N. Kamo. 2001. Environment around the chromophore in *pharaonis* phoborhodopsin: mutation analysis of the retinal binding site. *Biochim. Biophys. Acta.* 1515:92–100.

Shimono, K., M. Iwamoto, M. Sumi, and N. Kamo. 1997. Functional expression of pharaonis phoborhodopsin in *Escherichia coli. FEBS Lett.* 420:54–56.

Shimono, K., M. Iwamoto, M. Sumi, and N. Kamo. 2000. Effects of three characteristic amino acid residues of *Pharaonis phoborhodopsin* on the absorption maximum. *Photochem. Photobiol.* 72:141–145.

Spudich, J. L. 1998. Variations on a molecular switch: transport and sensory signalling by archaeal rhodopsins. *Mol. Microbiol.* 28:1051–1058.

Spudich, J. L., C. S. Yang, K. H. Jung, and E. N. Spudich. 2000. Retinylidene proteins: structures and functions from Archaea to Humans. *Annu. Rev. Cell Dev. Biol.* 16:365–392.

Subramaniam, S., and R. Henderson. 2000. Crystallographic analysis of protein conformational changes in the bacteriorhodopsin photocycle. *Biochim. Biophys. Acta.* 1460:157–165.

Sudo, Y., M. Iwamoto, K. Shimono, M. Sumi, and N. Kamo. 2001. Photo-induced proton transport of pharaonis phoborhodopsin (sensory rhodopsin II) is ceased by association with the transducer. *Biophys. J.* 80:916–922.

Takao, K., T. Kikukawa, T. Araiso, and N. Kamo. 1998. Azide accelerates the decay of M-intermediate of pharaonis phoborhodopsin. *Biophys. Chem.* 73:145–153.

Wegener, A. A. 2000. Untersuchungen zur Wechselwirkung des archaebakteriellen Lichtrezeptors pSRII mit seinem Transducerprotein pHtrII. Dissertation, University of Dortmund, Germany.

Wegener, A. A., I. Chizhov, M. Engelhard, and H. J. Steinhoff. 2000. Time-resolved detection of transient movement of helix F in spin-labelled pharaonis sensory rhodopsin II. *J. Mol. Biol.* 301:881–891.

Wittenberg, R. 1995. Charakterisierung der Elektronentransportkette und Untersuchungen zur Bioenergetik in *Natronobacterium pharaonis*. Dissertation, Ruhr-Universität, Bochum, Germany.

Zhang, W. S., A. Brooun, M. M. Mueller, and M. Alam. 1996. The primary structures of the archaeon *Halobacterium salinarium* blue light receptor sensory rhodopsin II and its transducer, a methyl-accepting protein. *Proc. Natl. Acad. Sci. U. S. A.* 93:4649–4654.